

Received November 14, 2018, accepted December 5, 2018, date of publication December 18, 2018, date of current version January 23, 2019.

Digital Object Identifier 10.1109/ACCESS.2018.2887228

# Application of Tiling Theory for Path Planning Strategy in a Polyiamond Inspired Reconfigurable Robot

RIZUWANA PARWEEN<sup>ID</sup>, VEERAJAGADHESWAR PRABAKARAN<sup>ID</sup>, MOHAN RAJESH ELARA<sup>ID</sup>,  
AYYALUSAMI VENGADESH<sup>ID</sup>, AND VINU SIVANANTHAM

Engineering Product Development, Singapore University of Technology and Design, Singapore 487372

Corresponding author: Rizuwana Parween (rizuwana\_parween@sutd.edu.sg)

This work was supported by the National Robotics Research and Development Programme Office (NR2PO) Singapore.

**ABSTRACT** Commercial floor cleaning robots face significant challenges in accessing convex and narrow corners due to their fixed and regular morphologies. To overcome this, we develop a new class of self-reconfigurable floor cleaning robot, hTetrakis, which is composed of tetriamonds (four equilateral triangles aligned along the edges) that adopt three distinct forms (“I”, “A”, and “U” shapes). When on a flat and rigid platform, these forms have convex corners that help to cover narrow regions. This paper addresses the mechanical structural design, reconfiguration of the robot platform through the hinge mechanism, and the electronics and navigation module of hTetrakis. Based on finite element studies, we estimate the system’s natural frequency, stress, and deformation patterns developed in the structural components of the robot, and validate the proposed design to overcome structural failure and system resonance. In order to achieve maximum area coverage using the tetriamond forms, we formulate tiling theorems and apply them for path-planning techniques during the floor cleaning process. By using a robot prototype, we conduct experiments to validate the proposed tiling theorem based on the percentage of area coverage, and demonstrate that this platform is able to cover the floor area efficiently.

## INDEX TERMS

Coverage area, path planning strategy, polyiamond tiling theory, reconfigurable floor cleaning robots.

## I. INTRODUCTION

Cleaning large floor areas using traditional cleaning methods (mopping, brooming, vacuum cleaning) is a tedious and unpleasant process as it requires huge manpower that involves tremendous effort and time. Over the last decade, advancements in software technology, artificial intelligence, hardware, and imaging techniques have helped researchers to develop floor-cleaning robots for domestic and commercial settings. As per the current market survey, iRobot, Samsung, Neato, and Dyson are the dominant suppliers of floor-cleaning robots. They adopt an autonomous navigation system that maps the environment and follows various path-planning algorithms to cover floor areas and navigate obstacles by using integrated sensors. These robots are usually lightweight, easy to move around the home and commercial places, and able to clean floors without human intervention. These robots liberate human operators from the unpleasant

task of cleaning, reduce overall cleaning time, and improve the overall effectiveness of the cleaning process. However, due to the fixed morphologies (circular or D-shaped) of existing commercial robots, they cannot reach all narrow spaces and sharp regions among obstacles in normal cleaning environments. To overcome these issues, the research community has started developing modular and self-reconfigurable floor cleaning robots over the past few years. Our previous work on the hTetro robot, which represents a novel self-reconfigurable floor cleaning robot inspired by the famous Tetris game.

The hTetro robot is one of the recent advancements within the area of modular reconfigurable floor cleaning robots [1], [2]. This robot is capable of transforming between any of the seven one-sided Tetris pieces, with the objective of maximizing the area coverage. We validated the efficiency of the proposed robot in terms of area coverage by benchmarking its performance with two fixed morphology robots.

The hTetro could demonstrate superior area coverage performance than the robot with two fixed morphologies by changing its morphology with respect to the sensed environment. It is critical for robots that are developed and deployed for cleaning applications to achieve efficient coverage path planning. Path planning is a method that regulates the robot's path, allowing it to pass over all parts of an area while avoiding obstacles. Over the past few decades, various path planning methods have been proposed and demonstrated on robots with numerous applications. One of the most frequently used path-planning methods is cellular decomposition, which breaks the obstacle-free areas into a non-overlapping region. These regions are called 'cells,' which are easy to cover and require only simple motions (e.g., zigzags) to sweep an entire area. Previous studies have documented the generation of simple motions using the cellular decomposition method [3]–[5]. However, Choset *et al.* [6] proposed a new approach called boustrophedon cellular decomposition which works similarly to other decomposition methods. However, the proposed method reduced the number of cellular cells compare to the trapezoidal algorithm; hence, a shorter coverage path is obtained by robots. Furthermore, Galceran and Carreras [7] presented a coverage path plan method based on the Morse decomposition function for an underwater surface robot. That work determined the optimal sweep orientation for each separated cell and the inter-lap spacing in the generated path on a lap-by-lap basis with respect to the ocean depth. Moreover, they validated the proposed algorithm in simulation experiments with real-time bathymetric data sheets. An alternative algorithm for the Morse decomposition method was proposed in [8], who presented a landmark-based topological coverage in which the natural landmarks are added as nodes in the mapped space. In addition, the authors bench-marked their proposed path-planning approach with the Morse based method and demonstrated higher coverage performance with the proposed scheme.

The utilization of grid-based methods for coverage path planning opens numerous opportunities for research and development in the field of robot navigation. Many such algorithms have been proposed for efficient path planning for mobile robots. For Instance, Baek *et al.* [9] presented a novel grid-based coverage approach where they considered time and energy as a critical parameter for reducing directional constraints on path generation. The proposed approach was validated by benchmarking its performance in conventional coverage schemes with respect to energy and time. For multi-robot coverage, Fazli *et al.* [10] proposed a multi-robot area coverage approach for a scenario where a map is known with the minimum visibility range. In this work, authors initially located the beacons in a known map to create a graph. Then, they converted the generated graph into a forest of partial spanning tree (PST). The converted PST is then built as cycles, which are then assigned to each robot for coverage. Although numerous methods in coverage path planning have been proposed and demonstrated, they have

primarily been tested with fixed morphological robots in area coverage tasks. None of the previous works in coverage path planning have been applied or proposed explicitly for robots with shape-shifting capabilities. Moreover, it is difficult to utilize the existing area coverage technique to shape-shifting robots due to their ability to change morphologies, which varies the kinematic and dynamic models of the concerned robots, thereby affecting its control parameters during navigation.

In our previous work, we proposed a coverage technique for a polyomino robot class that consists of three blocks called hTromo [11], and applied polyomino tiling theory developed hTromo robot as a means of solving the area coverage problem. We validated five different tiling theorems with this robot, and the results indicated that the efficacy of the proposed approach produces a higher level of area coverage performance. The proposed technique acts as a path-planning scheme for all class of polyomino-based reconfigurable robots. Although robots that were developed under the polyomino principle demonstrated exceptional area coverage performance, they are explicitly designed for impartial spaces. The polyomino robots consist of square blocks wherein the system can perform better in an impartial area [12]–[14]. However, performance degradation can occur if it is deployed in a non-parallelogram structured space. By applying specific combinatorial properties to polyominoes, we obtain the finite number of simple graphs, which are limited to rectangular regions. Polyominoes never form the graphs of convex polyforms. The reason why polyforms cannot be the vertex-edge graph of 3-D polyforms is that any connected finite figure composed of squares will have boundary corners. However, polyiamonds are a category of polyform joining two or more similar equilateral triangles along the edges [15]. With polyiamonds, we obtain a larger variety of geometric figures than the polyominoes. To date, polyiamond-based tiling theory has not been used to cover the sweeping region of reconfigurable floor-cleaning robots.

The omni-directional wheels are used for this platform locomotion as these wheels are capable of moving freely in any direction in two-dimensional space which implies these wheels have three degrees of freedom. The omni-directional wheel provides greater flexibility as it is able to adapt the linear and self-turning motion in any direction. It helps the platform to achieve the obstacle avoidance and trajectory tracking quickly. However, it needs a robust motion control algorithm that guarantees the smooth movement of the platform during navigation. Numerous research has been conducted towards the motion control of the omni-directional wheel based mobile robots [16]–[20]. Different motion control schemes including sliding-mode control [21], neural-networks [22], fuzzy network [23]–[25], fuzzy wavelet network [26], proportional-integral-derivative (PID) based controller [27], [28] have been used. However, this present platform has the locomotion either along the straight lines (either X or Y direction) or the self-turning about the Z-axis.

Therefore, two levels of simplified PID controller have been used for this platform.

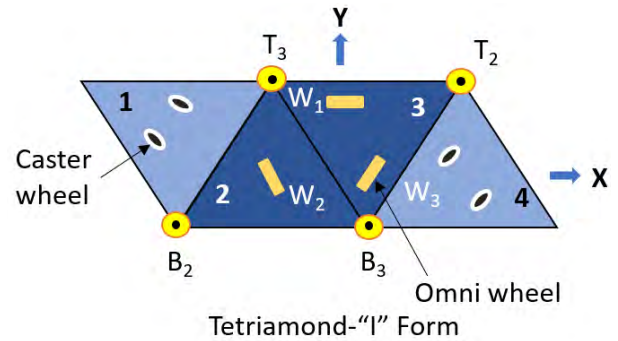
In this paper, we present a counter design for the polyomino class of robot, called hTetrakis, that consists of four equilateral triangular blocks linked with two hinged points. This robot is designed under the principle of polyiamond. The objective of this reconfigurable robot is to generate complex and irregular configurations which are essential for achieving the necessary modularity to perform various tasks, which is out of the reach of the single module. It addresses the mechanical architecture, reconfiguration mechanism of the robot platform through the hinge mechanism, and electronics, motion control scheme and navigation module of the robot. In addition, by using finite element analysis, both static and modal analysis are carried out. Based on the finite element studies, the system's natural frequency, stress and deformation patterns developed in the structural components of the robot are estimated. For efficient area coverage, various path planning theorems based on polyiamond tiling theory are proposed. By using the robot prototype, experiments are carried out to validate the proposed tiling theorems.

## II. ROBOT ARCHITECTURE

hTetrakis is a self-reconfigurable wheeled robot consisting of four triangular blocks. Each triangular block is the fundamental unit of this robotic system and plays an important role during system reconfiguration. It adapts to the cleaning environment by changing its configuration according to the obstacle present. Therefore, the structural design of the fundamental unit is essential for achieving its function and modularity. Based on the functionality, this robotic system consists of hinged, locomotion, structural, and control modules. We use an ultra-wideband (UWB)-based radio navigation system for robot operation that measures the distance and location of the robot to an accuracy of 5 to 10 cm and consumes significantly less power. Arduino Atmega 2560 16-bit microcontroller is used for reconfiguration, mobility, control, and Bluetooth connectivity for full-duplex serial communication. The user interacts with the robot's microcontroller via the Bluetooth communication interface. The microcontroller receives commands from the Arduino and processes that by sending pulse width modulation signals to the motor unit.

### A. DESIGN OF HINGE JOINT

For efficient cleaning, the hTetrakis robot must move instantly in any direction on the platform when it comes in contact with obstacles. The robot platform is designed to have three degrees of freedom on the XY planar surface (translation along X and Y-direction, rotation about Z-direction). Due to the restricted in-plane movement, the blocks must be connected using a revolute joint with the joint axis being along the Z-axis. As the objective is to obtain all three ('A', 'I', and 'U') tetriamond forms during the reconfiguration process, we place the joints either at the  $T_3$  and  $T_2$  location along the top edge or at  $B_3$  and  $B_2$  joints along the bottom edge, as shown in Fig. 1.  $T_3$  and  $T_2$  represent the joints

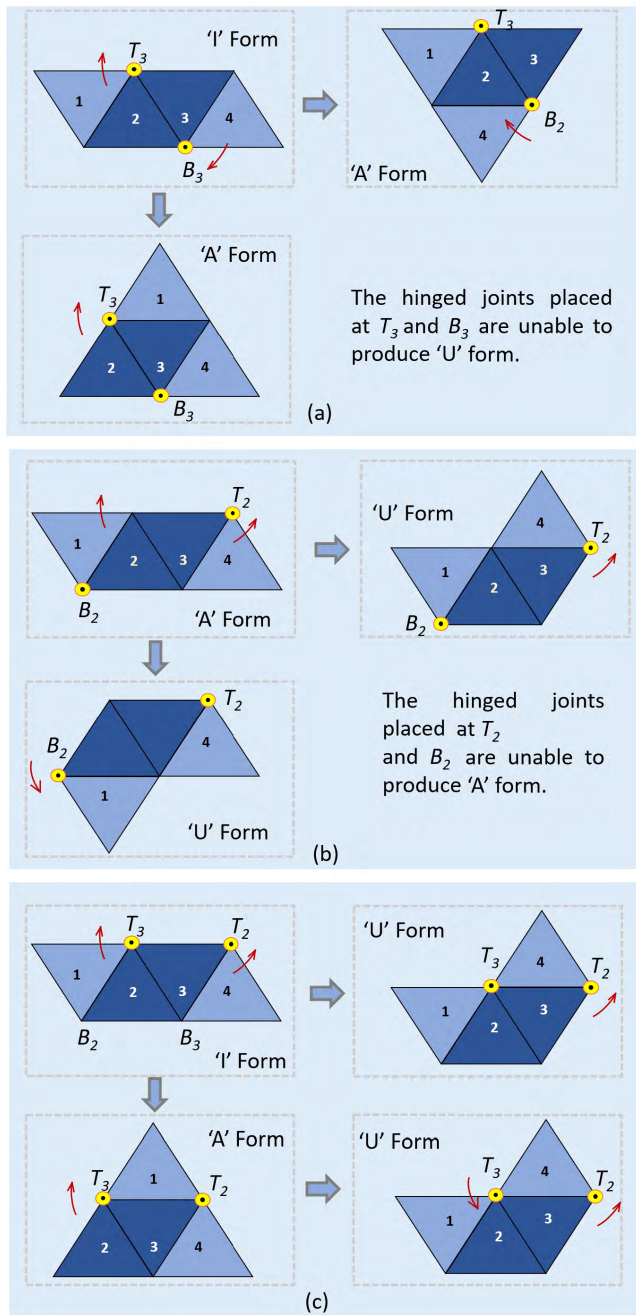


**FIGURE 1.** Tetriamond 'I' form showing the joints at  $T_3$  and  $T_2$  location along the top edge or at  $B_3$  and  $B_2$  location along the bottom edge.

connecting three and two blocks, respectively. Similarly,  $B_3$  and  $B_2$  represent the joints along the bottom edge connecting two blocks and three blocks, respectively. If we place the revolute joints at  $T_3$  and  $B_3$ , we obtain only 'A' and inverted 'A' forms due to the rotation of block '4' at  $T_3$  and block '1' at  $B_3$  joint location, shown in Fig. 2(a). Similarly, if we place the revolute joints at  $T_2$  and  $B_2$ , we obtain only 'U' form due to the rotation of block '4' at  $T_2$  or block '1' at  $B_2$  joint location, as shown in Fig. 2(b). However, if we place the revolute joints at  $T_2$  and  $T_3$ , we obtain both 'A' and 'U' forms due to the rotation of block '4' at  $T_2$  and block '1' at the  $T_3$  location, respectively, as shown in Fig. 2 (c). Among these, we apply the third layout for placing the revolute joints (as it can adapt all of the these forms) and propose the mechanical design of the robot.

In the previous section, we highlighted that the second and third blocks participate only in locomotion (not in reconfiguration). Therefore, we consider these two blocks as static blocks and mount them on three plastic Omni-wheels of 58 mm diameter (maximum 50 rpm) at the center of the block, as shown in Fig.1. The Omni-wheels are designed in such a way that they can rotate and move the platform in multiple directions [31]. We place the axes of these wheels at an incline of 120 degrees to each other. We apply the principle of the parallelogram law of vector addition to the forward and reverse wheel directions of the three Omni-wheels to obtain the resultant locomotion of the robot along X (translational), Y (translational), or Z (rotation) direction. For the forward motion of the wheels,  $W_2$  and  $W_3$ , ( $W_1$  spin about their axis) the robot travels in Y-direction. Similarly, for the forward motion of the wheels,  $W_1$  and  $W_3$  and reverse motion of the wheel  $W_2$ , the robot travels in X-direction. To have static and dynamic stability of the robot, each block must not overturn. Therefore, we placed all structural and electronic parts in a distributed manner so that the center of mass always lies within the support polygon (i.e., the polygon connecting all of the wheel positions at the base of the robot) [33]. The first and fourth blocks turn around the hinge joint during reconfiguration. To ensure stable locomotion and shape-shifting, we mount both blocks (1 and 4) on castor wheels. In order to achieve free motion of the connecting blocks at the hinge, we filleted each edge.

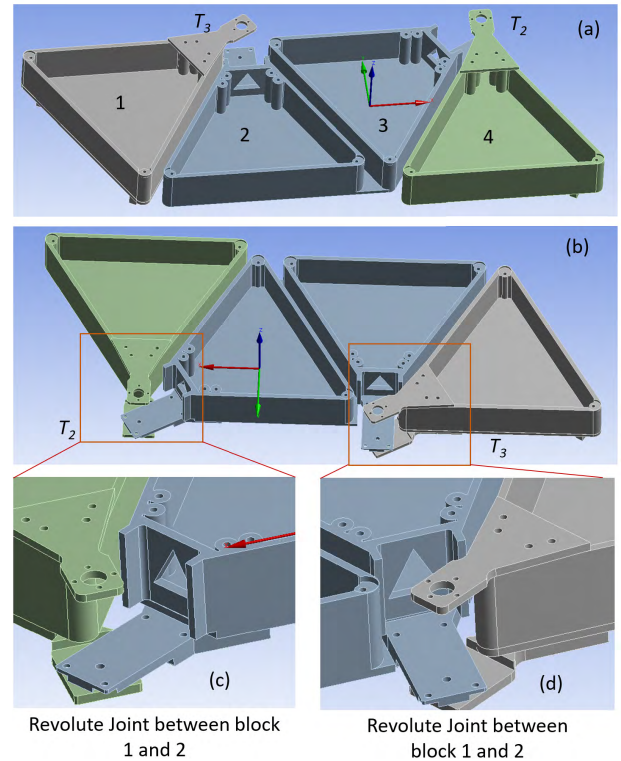




**FIGURE 2.** Reconfiguration from 'I' form to 'A' and 'inverted A' forms using revolute joint at  $T_3$  and  $B_3$  locations, (b) Reconfiguration from 'I' form to 'U' forms using revolute joints at  $T_2$  and  $B_2$  locations, (c) Reconfiguration from 'I' form to 'A' and 'U' forms using revolute joints at  $T_3$  and  $T_2$  locations.

**B. STRUCTURAL AND ELECTRONICS MODULE**

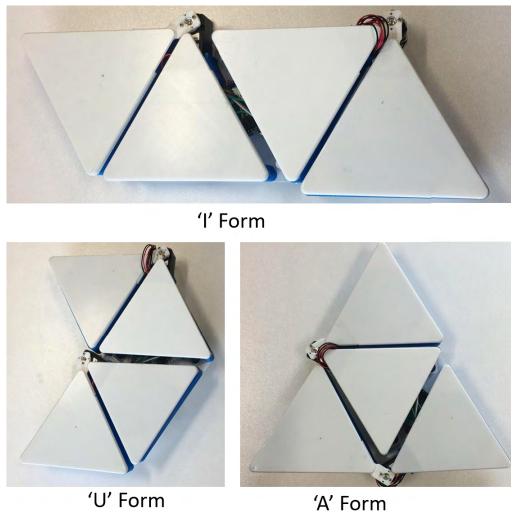
Each triangular block of hTetrakis platform is of 140 mm. We selected the height of each block as 50 mm to accommodate the electronics hardware components and motors. These blocks also carry all the cleaning accessories and wheels for locomotion and reconfiguration. Figure 3 (a) and (b) present the 3D CAD model of the hTetrakis robot. Block 1 is attached to block 2, while block 4



**FIGURE 3.** The 3D CAD model of the hTetrakis robot showing (a) front view, (b) back view, (c) the revolute joint at  $T_3$ , and (d) the revolute joint at  $T_2$ .

is attached to block 3 using hinges. Figure 3 (c) and (d) present the detailed design of the revolute joints of the robots. We mounted Herkulex drrs 0201 servo motors on the hinges that drive block 1 and block 4 during transformations. Each servo motor has a voltage rating of 7.4 V and a standby stall torque of 24 kg cm which sufficient to drive the blocks and make transformations. The locomotion (translation and rotation) of the robot is performed by blocks 2 and 3, which are mounted with DC motors (M1, M2, and M3) and Omni-wheels. The whole arrangement of the wheels is in triangular structure with an internal angle placement of 60 degrees each.

For motor's rotational speed (under load) of 30 rpm, the maximum attainable translational speed ( $\pi \times \text{diameter} \times \text{speed in rps}$ ) of the robot is approximately 90 mm/sec. If the robot reaches this maximum speed in 3 sec on flat terrain, then the acceleration is  $30 \text{ mm/sec}^2$ . We consider the total weight of the robot as 2.5 kg including the structural, control and cleaning accessories. The torque (mass  $\times$  acceleration  $\times$  wheel radius/ Number of wheels) [32] required by the motor to drive this load (2.5 Kg) at acceleration of  $30 \text{ mm/sec}^2$  over two sets of active wheels is 1.8 Nmm. The stall torque of the motor must be more than the torque required to drive the load. Therefore, we selected a plastic-gearred DC motor (90 degree output, with a gear ratio of 200:1) with a voltage rating of 6 V, a rotational speed as 51 rpm, and a maximum torque of 706 Nmm, which is more than the total torque needed to drive the load. We used pulse width modulation to drive.



**FIGURE 4.** The prototype of the hTetrakis showing various shapes 'I', 'A', and 'U'.

In addition to the Omni-wheels, we used two caster wheels on blocks 1 and 3 for reconfiguration. Moreover, we fabricated the structural module, motor housing, and hinged joint component with polylactic acid (PLA) material using a Cubicon 3D printer, as shown in Fig. 4.

### C. NAVIGATION SYSTEM

The communication architecture diagram of hTetrakis is shown in Fig. 5, which consists of a navigation system, a master controller and the robot platform. The primary purpose of the navigation system is to provide streaming sensor data to the controller. The navigation sensors consist of multiple transmitters and a receiver, which will be placed on the hTetrakis platform. Once the robot navigation begins, the system calculates the distances between sensors and streams the data to the master controller in real time. The master controller is in charge of several crucial tasks for the overall system to operate. Once the distance data from the navigation system is received, the robot localization algorithm will calculate the robot position based on trilateration, which is a commonly used process that determines the absolute coordinate of points based on distance measurements. The estimated position results are saved in a data log and are further used by the robot's decision-making algorithm. In order to navigate the robot to a specific coordinate within the workspace while preventing any collisions with obstacles, a path-planning algorithm is implemented in the master controller. The off-line path-planning algorithm generates a series of waypoints before the navigation process begins. Each waypoint indicates a specific coordinate in the workspace and the hTetrakis morphology. The waypoint series generated by the path planner form a consecutive path within the environment such that the area covered by hTetrakis blocks throughout the navigation process is maximized.

The robot decision-making algorithm will be in charge of locomotion of the hTetrakis platform during the

navigation process. It takes real-time estimated robot position data and the waypoint series as inputs, and then calculates the distance between the current position of the robot and the ideal waypoint position. If the distance is within an allowed threshold value with the correct hTetrakis morphology, the waypoint would be considered as 'cleared' and a new waypoint will be designated. Otherwise, linear motion commands will be sent whenever the robot position deviates too far from the ideal position, and shape-shifting commands will be sent under situations where the current morphology differs from the required morphology of the next waypoint. All commands are transferred through Xbee devices between the master controller and the hTetrakis robot platform. Once the robot platform receives commands from the master controller, the micro-controller on the robot will decipher the codes and perform the corresponding actions. State machines are being implemented into the platform so that even a single instruction (such as a command to move forward) will result in a different combination of motors being activated based on the current hTetrakis morphology. Several other sensors, including an inertial measuring unit (IMU), are also being implemented into the platform for the hTetrakis robot to automatically correct its orientation to secure better overall performance throughout the navigation process.

### D. MOTION CONTROL

The schematics of control architecture for this reconfigurable platform is illustrated in Fig. 6. The control architecture consists of a master control system to control the locomotion and shape shifting during reconfiguration. This master controller has two sub-control layers, i.e., Layer A for shape shifting and Layer B for controlling the locomotion. Layer A is responsible for sending set point command to the platform. The platform use this set point command for 'shape shifting' of platform as per the environment. This layer has a PID controller with feedback about the angular position of the hinged joint. The encoders mounted at the joint measures the joint angle and velocities. The proposed control law estimates the error between the reference and actual angular position and velocities, and then computes the joint torques which is a function of error signal using the proposed dynamic model of the reconfiguration process, and maintains a bounded steady state error. After finalising the shape, layer A takes the decision on control inputs on the particular shape and gives input about the platform shape, the joint angle, torque to the layer B. Layer B has a computed torque based PID controller to nullify the external disturbances during heading and zero-pivoting and follow the desired trajectory. The control law incorporated in layer ensure that the mobile robot can track target trajectory. Its obvious that the control algorithm will become more and more complex with the number of monoiamond increases. However, the current design decouples the structural unit of the reconfiguration and locomotion unit hence, the above simplified control scheme is able to achieve the objective.

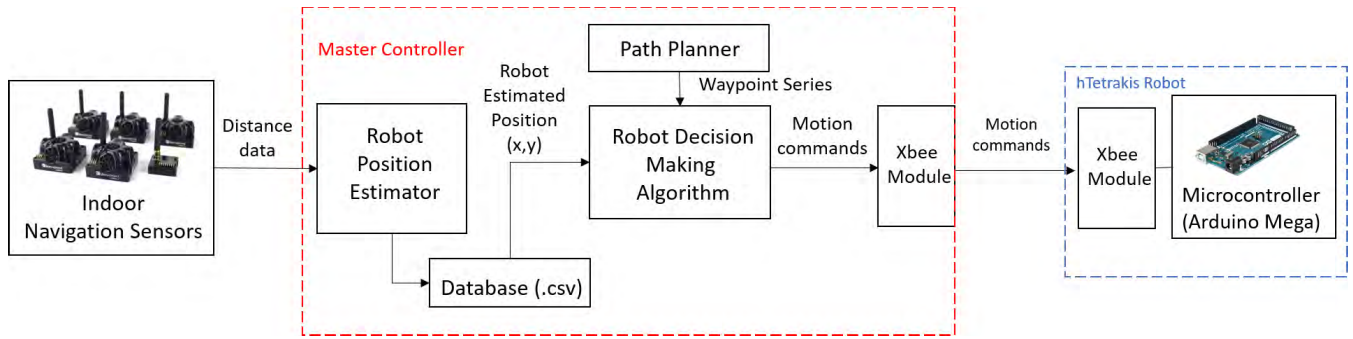


FIGURE 5. Navigation system architecture of hTetrakis platform.

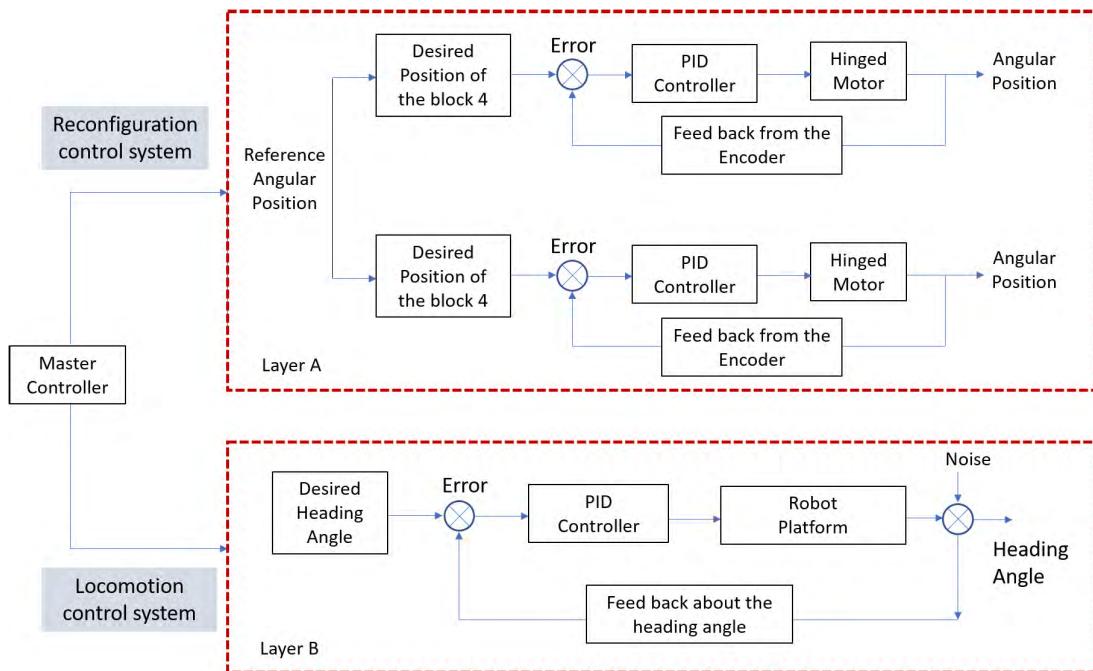


FIGURE 6. Control architecture of the hTetrakis.

III. FINITE ELEMENT BASED MODELING

The hTetrakis robot represents a dynamical system driven by electric motors. The system must be designed with a driving frequency (or wheel rpm) less than the natural frequency of the system so that the system overcomes resonance. We used the Finite Element (FE) package for ANSYS Workbench to perform a frequency (modal) analysis of the robot model [36], [37]. First, we built the CAD model in Solidworks and imported the model to ANSYS workbench environment. We assigned the density, poisson ratio, and Young’s modulus of PLA as 1.24 g/cm<sup>3</sup>, 0.3, and 3.36 GPa to the model, respectively. We added the total mass of the cover, electronics modules and cleaning accessories as 2.5 kg of distributed load over the base of the entire robot. We discretized the 3D model with the Solid187 element, which is a ten-noded solid 3D element with three degrees of freedom at each node translation in the X, Y, and Z direction, which thus

takes quadratic displacement behavior into account. Based on the convergence check, we set the element edge size as 1 mm. The meshed FE model of the robot, containing the total number of elements as. At the wheel location, the robot is free to translate and rotate in the XY plane, though is constrained along the Z-axis. Hence, at the wheel support region, we consider the degree of freedom including X and Y rotation (out-of-plane) and Z translation as zero. With this boundary setting, we conducted a modal (free vibration analysis) using the Block Lanczos modal extraction method to obtain the natural frequencies and mode shapes of the robot structure. We obtained the first three natural frequencies as zero, which implies that these three modes are the rigid body modes. The first, second, and third mode shapes showed the rigid body translation along X, rigid body translation along Y, and rigid body rotation along the Z axis. These are the trivial modes as the robot is not fixed rigidly. However, we obtained the fourth



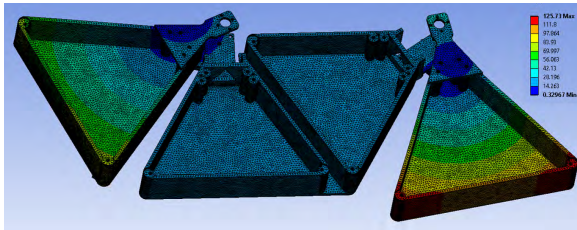


FIGURE 7. The fourth mode shape of the robot structure.

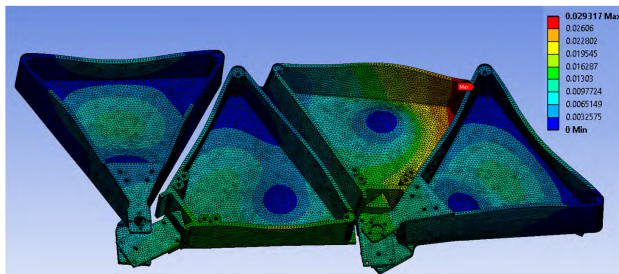


FIGURE 8. The deformation pattern due to gravitational load in robot structure.

natural frequency as 72 Hz, which demonstrates the in-plane bending of block 1 and block 4 with respect to block 2 and block 3, as shown in Fig. 7. The driving frequency of the robot during the locomotion and reconfiguration processes must be less than this natural frequency to avoid structural failure under resonance. During locomotion and reconfiguration, the operating speed of the motor DC motor is 20 rpm (0.3 Hz), thus the robot structure represents a safe design

The mechanical load in this self-reconfigurable robot includes the gravitational (1g) effect (self-weight of 2.5 kg including electronic components and cleaning accessories) and torque due to motor rotation. We applied the self-weight as a distributed load that spans uniformly across the surface of all the four boxes and fixed the structure at the wheel support, and then conducted a static structural analysis to obtain the deformation and stress pattern on the various components of the robot. Figure 8 shows the deformation pattern of the robot under the above mentioned loading conditions. The maximum deformation is 0.027 mm, which occurs near the distant edge of block 1 and 4. This deformation is less than the one-tenth of the critical dimension, hence it is in the allowable limit. Figure 9 presents the distribution of the principal stress in the robot structure. Maximum stress occurs near the wheel support and the motor holder attached to the joint. Studies indicate that the failure of the 3D-printed parts made of PLA is similar to brittle material [34], [35]. Hence, we have used the maximum stress criterion to predict the failure of brittle materials. As per this criterion, the failure occurs when the maximum principal stress reaches the uniaxial tension strength. The tensile stress of the PLA is 40 Mpa. It is clearly evident from the stress pattern that the maximum stress is 0.7 N/mm<sup>2</sup>, which is lower than the tensile stress of PLA. Therefore, the design is considered safe. However, the local-

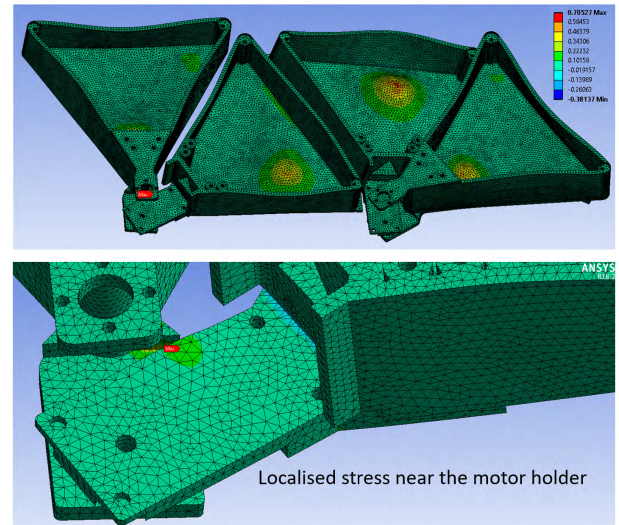


FIGURE 9. The distribution of the principal stress in robot structure.

ized maximum stress near the wheel support is mainly due to the concentrated loading and sharp corners. By adding fillets near the edges of the wheel support, we can reduce the stress concentration.

#### IV. PATH PLANNING TECHNIQUES BASED ON COMBINATORIAL PROPERTIES OF POLYIAMOND

The polyiamond tiling theory deals with filling a geometrical region by joining multiple monoiamonds [29]. A monoiamond is a special type of polyform, and is an equilateral triangle with three vertices, at two degrees, as shown in Fig. 10. The degree of a vertex represents the number of triangles that can be connected along its adjacent edges. For example, in the case of monoiamonds, each vertex has two degrees. In the case of diamonds, vertices 1, 3 and 2, 4 have two and three degrees, respectively. Based on certain rules of combinatorial properties, we obtain various two-dimensional geometric patterns by aligning the equilateral triangles together along the edge. The rules are as follows [30].

- Each monoiamond can connect with the other monoiamond along one its edge. They must share the entire edge (no partial sharing is allowed).
- The triangles are not allowed to connect at other triangles (except at the vertex) as it leads to unbalanced forms.
- If we add a monoiamond by joining along one edge, then the vertex that is adjacent to the other two edges will be new, and we have added one new vertex. The two vertices of the added edge will have their degrees increase by one through the addition of the triangle.
- If the triangle is added to an existing figure that shares two edges with the pre-existing figure, then this has been accomplished by drawing an edge between two vertices of the existing figure. No new vertex is added.
- If the triangle added to an existing figure that shares three edges, then this amounts to a hole


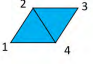




n	Form Name	Types of Forms
1	1-oiamond (Moniamond)	
2	2-oiamonds (Diamond)	
3	3-oiamonds (Triamond)	
4	4-oiamonds (Tetramond)	  

FIGURE 10. Different forms of planar polyiamonds (n-oiamonds).

existing in the figure that is now a constituent triangle.

- The geometric figure should not create a single missing monoiamond called ‘holes’.
- The minimum and the maximum degree of any vertex can only be two and six, respectively.

Based on the number of monoiamond joined together, the geometric patterns are classified into diamonds (2-monoiamonds), triamonds (3-monoiamonds), tetramonds (4-monoiamonds), pentiamonds (5-monoiamonds), and hexiamond (6-monoiamonds), shown in Figure 10. By rearranging the alignments of the triangles along the different edges, we obtain the finite number of configurations. For example, diamonds and triamonds have only one configuration. However, tetramonds, pentiamonds and hexiamonds have three, four, and twelve configurations, respectively. The tetramond has three distinct forms, i.e., ‘I’, ‘A’, and ‘U’. These obtained forms have convex boundary corners. The combinatorial properties of the polyiamonds are discussed below.

*Theorem 1:* A vertex can have a maximum of six degrees in order to complete a closure disk (six equilateral triangles make two angles). Therefore, we can construct a planar closure figure with multiple of n-oiamonds having vertices of between two and six degrees, while the generated figure cannot contain any holes if the vertices of the n-olyiamonds obey the vertex valency [30] shown in Equation(1)

$$2V_2 + V_3 = 6 + V_5 + 2V_{6ext} \tag{1}$$

*Theorem 2:* A parallelogram of size  $a \times b$  can be tiled with only ‘I’ set of tetramonds if (and only if) the total number of triangles ( $ab/2$ ) is a multiple of 4.

*Theorem 3:* A parallelogram of size  $a \times b$  can be filled with ‘A’ form completely if (and only if) the total number of triangles ( $ab/2$ ) is multiple of 8, and both  $a, b \geq 4$ .

*Theorem 4:* A parallelogram of size  $a \times b$  can be filled with both ‘I’ and ‘A’ forms completely if (and only if) the total number of triangles ( $ab/2$ ) is multiple of 12, and both  $a, b \geq 4$ .

*Theorem 5:* A parallelogram  $a \times b$  can be tiled with all the three forms i.e., ‘I’ and ‘A’ and ‘U’ set of tetramonds if (and only if) both  $a$  and  $b$  are multiple of 8.

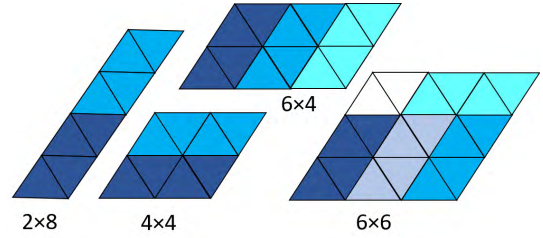


FIGURE 11. Tiling a parallelogram with ‘I’ form of the tetramond.

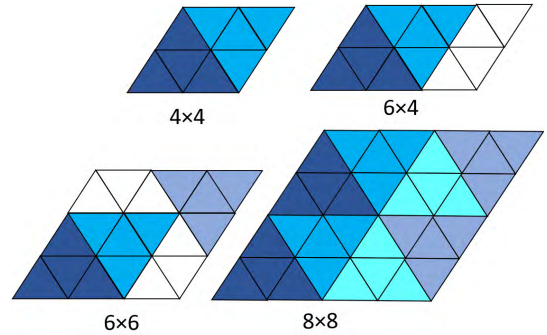


FIGURE 12. Tiling a parallelogram with ‘A’ form of the tetramond.

## V. AREA COVERAGE EXPERIMENTS BASED ON POLYIAMOND TILING THEORY

We assume the cleaning environment to be a large parallelogram of dimension  $A \times B$ , which is primarily due to the presence of obstacles (furniture or plants) at the corners.  $A$  (or  $B$ ) represents the number of triangles attached to the base of the parallelogram by the edge and vertex of the triangle. The number of triangles present in the  $A \times B$  parallelogram is given  $AB/2$ . In order to tile the  $A \times B$  parallelogram completely with all the three forms of the tetramond (‘I’, ‘A’, and ‘I’ sets) without any void, we can use the following decomposition techniques. Firstly, for efficient cleaning and tiling-based path-planning, we decompose the large parallelogram into many smaller-sized parallelograms of size  $a \times b$  in such way that the sides of both parallelograms are always parallel with each other. Secondly, we can tile the  $A \times B$  parallelogram completely with parallelograms of  $a \times b$  if both  $A$  and  $B$  are multiples of  $a$  and  $b$  respectively. For example, Figure 15 represents a large parallelogram of dimension  $16 \times 16$ . It can be filled with four  $8 \times 8$  parallelogram without any void. Each small parallelogram ( $a \times b$ ) can be tiled with any forms of tetramond as per the tiling theorem.

Each run of our experiment began with the hTetrakis robot being placed in a pre-defined initial position inside the testbed area. We recorded the robot in action from the beginning to the end of the experiments. Once the tests were completed, the recorded videos were post-processed to generate track maps using the image processing algorithm detailed in the previous paragraph. Figure 16 presents the track map images of the hTetrakis robot from the first set of experiments



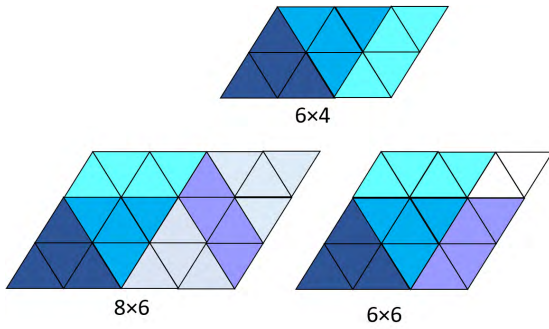


FIGURE 13. Tiling a parallelogram with 'A' and 'I' forms of the tetriamond.

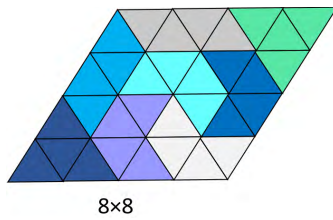


FIGURE 14. Tiling a parallelogram with all forms of the tetriamond.

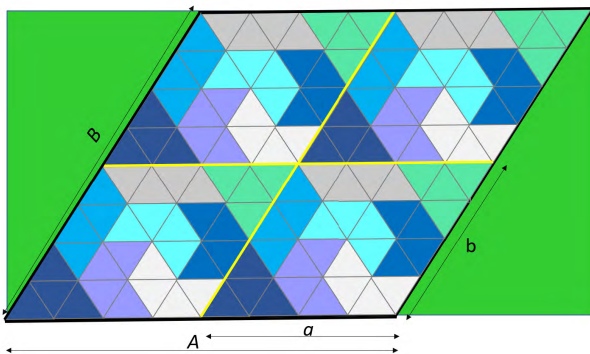


FIGURE 15. Tiling a parallelogram of size 16x16 with all forms of tetriamond.

involving the validation of Theorem 5. The green-colored shading represents the area covered by the robot. The percentage of area covered is displayed on top of the tracked images. We determined the percentage of area covered based on the tiling equation. Figure 16 presents the tiled area during different stages of our first set of experiments. This figure indicates the actual position of the robot at a specific instance in time and the associated track map at that instance is overlaid with the tiling set. The robot path was executed adhering to the global tiling set generated based on Theorem 5 (shown in Fig. 14).

## VI. CONCLUSION

We proposed a novel floor-cleaning robot that undergoes self-reconfiguration and is capable of dealing obstacles containing convex and sharp corners in static and dynamic environments. In this paper, we presented the robot architecture including

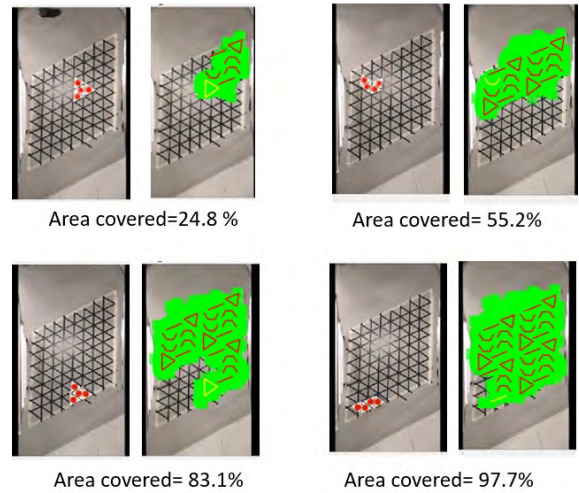


FIGURE 16. Experiments validating application of Theorem 5 on h-Tetrakis robot.

the structural design, locomotion, control and navigation system of the robot and tiling based path planning techniques for maximum area coverage during cleaning process. Firstly, based on static analysis of the FE model, we estimated the deformation and stress patterns in various components of the robot structure. We observed that stress and deformation were within the allowable limits, and hence we ensured that the structure has a safe design with respect to the actual loading condition. We determined the frequency and mode shape of the structure based on modal analysis, and set the driving frequency of the robot to 30 rpm (Hz), which is less than the 1st bending (4th mode) natural frequency of the system. Secondly, in order to ensure the maximum area of coverage during cleaning, we followed the path planning of this robot based on the tiling theory of polyiamonds. Based on the combinatorial properties of the polyiamond, we derived some theorems which were used for covering any parallelogram-shaped cleaning environment. Based on the design and FE analysis, we constructed the robot prototype and verified the proposed theorems for area coverage. We claim that the robot is able to reach every point at least once and cover the floor without any free space. It also generates configurations with sharp edges that can reach all convex and concave corners presented by obstacles, while also being able to reach under low labeled objects. Our future research involving the hTetrakis robot will focus on the development of path planning based on maximum area coverage and minimum navigation energy through an investigation of the actual cleaning ability of the robot with the integration of cleaning accessories, a control system based on the kinematics and dynamics of this platform.

## REFERENCES

- [1] V. Prabhakaran, M. R. Elara, T. Pathmakumar, and S. Nansai, "hTetro: A tetris inspired shape shifting floor cleaning robot," in *Proc. IEEE Int. Conf. Robot. Autom. (ICRA)*, May/Jun. 2017, pp. 6105–6112.

- [2] V. Prabhakaran, M. R. Elara T. Pathmakumar, and S. Nansai, "Floor cleaning robot with reconfigurable mechanism," *Automat. Construction*, vol. 91, pp. 155–165, Jul. 2018.
- [3] V. J. Lumelsky, S. Mukhopadhyay, and K. Sun, "Dynamic path planning in sensor-based terrain acquisition," *IEEE Trans. Robot. Autom.*, vol. 6, no. 4, pp. 462–472, Aug. 1990, doi: [10.1109/70.59357](https://doi.org/10.1109/70.59357).
- [4] H. Choset and P. Pignon, "Coverage path planning: The boustrophedon decomposition," in *Field and Service Robotics*. London, U.K.: Springer, 1998, pp. 203–209.
- [5] E. U. Acar, H. Choset, A. A. Rizzi, P. N. Atkar, and D. M. Hull, "Morse decompositions for coverage tasks," *Int. J. Robot. Res.*, vol. 21, pp. 331–344, Apr. 2002, doi: [10.1177/027836402320556359](https://doi.org/10.1177/027836402320556359).
- [6] H. Choset, E. Acar, A. A. Rizzi, and J. Luntz, "Exact cellular decompositions in terms of critical points of Morse functions," in *Proc. ICRA. Millennium Conf. IEEE Int. Conf. Robot. Automat. Symp.*, vol. 3, Apr. 2000, pp. 2270–2277.
- [7] E. Galceran and M. Carreras, "Efficient seabed coverage path planning for ASVs and AUVs," in *Proc. IEEE/RSJ Int. Conf. Intell. Robots Syst.*, Oct. 2012, pp. 88–93.
- [8] S. C. Wong and B. A. MacDonald, "A topological coverage algorithm for mobile robots," in *Proc. IEEE/RSJ Int. Conference Intell. Robots Syst. (IROS)*, vol. 2, Oct. 2003, pp. 1685–1690.
- [9] T. K. Baek, S.-H. Choi, S.-Y. Oh, and T.-K. Lee, "Smooth coverage path planning and control of mobile robots based on high-resolution grid map representation," *Robot. Auto. Syst.*, vol. 59, pp. 801–812, Oct. 2011, doi: [10.1016/j.robot.2011.06.002](https://doi.org/10.1016/j.robot.2011.06.002).
- [10] P. Fazli, A. Davoodi, P. Pasquier, and A. K. Mackworth, "Complete and robust cooperative robot area coverage with limited range," in *Proc. IEEE/RSJ Int. Conf. Intell. Robots Syst.*, Oct. 2010, pp. 5577–5582.
- [11] V. Prabhakaran, R. E. Mohan, V. Sivanantham, T. Pathmakumar, and S. S. Kumar, "Tackling area coverage problems in a reconfigurable floor cleaning robot based on polyomino tiling theory," *Appl. Sci.*, vol. 8, no. 3, p. 342, 2018.
- [12] C. S. Kaplan, *Introductory Tiling Theory for Computer Graphics* (Synthesis Lectures on Computer Graphics and Animation). San Rafael, CA, USA: Morgan & Claypool, 2009, pp. 1–113.
- [13] E. D. Demaine, M. L. Demaine, D. Eppstein, G. N. Frederickson, and E. Friedman, "Hinged dissection of polyominoes and polyforms," *Comput. Geometry*, vol. 31, pp. 237–262, Jun. 2005.
- [14] C.-W. Jho and W.-H. Lee, "Video puzzle game application of polyomino re-tiling," in *Embedded and Multimedia Computing Technology and Service*, vol. 181. Dordrecht, The Netherlands: Springer, 2012, pp. 363–369.
- [15] H. Fukuda, C. Kanomata, N. Mutoh, G. Nakamura, and D. Schattschneider, "Polyominoes and polyiamonds as fundamental domains of isohedral tilings with rotational symmetry," *Symmetry*, vol. 3, no. 4, pp. 828–851, 2011, doi: [10.3390/sym3040828](https://doi.org/10.3390/sym3040828).
- [16] T. Kalmár-Nagy, R. D'Andrea, and P. Ganguly, "Near-optimal dynamic trajectory generation and control of an omnidirectional vehicle," *Robot. Auton. Syst.*, vol. 46, pp. 47–64, Jan. 2004.
- [17] K. Kanjanawanishkul and A. Zell, "Path following for an omnidirectional mobile robot based on model predictive control," in *Proc. IEEE Int. Conf. Robot. Autom.*, May 2009, pp. 3341–3346.
- [18] H.-C. Huang and C.-C. Tsai, "Adaptive trajectory tracking and stabilization for omnidirectional mobile robot with dynamic effect and uncertainties," *IFAC Proc. Volumes* vol. 41, no. 2, pp. 5383–5388, 2008.
- [19] J. M. Ortíz and M. Olivares, "Trajectory tracking control of an omnidirectional mobile robot based on MPC," in *Proc. IEEE 4th Latin Amer. Robot. Symp. (Lars)*, Monterrey, Mexico, Nov. 2007, pp. 8–9.
- [20] G. I. R. K. Galgamuwa, L. K. G. Liyanage, M. P. B. Ekanayake, and B. G. L. T. Samaranyake, "Simplified controller for three wheeled omnidirectional mobile robot," in *Proc. IEEE 10th Int. Conf. Ind. Inf. Syst. (ICIIS)*, Peradeniya, Sri Lanka, 2015, pp. 314–319.
- [21] J. Mu, X.-G. Yan, B. Jiang, S. K. Spurgeon, and Z. Mao, "Sliding mode control for a class of nonlinear systems with application to a wheeled mobile robot," in *Proc. 54th IEEE Conf. Decis. Control (CDC)*, Osaka, Japan, Dec. 2015, pp. 4746–4751.
- [22] Z. Li, Y. Wang, X. Song, and Z. Liu, "Neural adaptive tracking control for wheeled mobile robots," in *Proc. Int. Conf. Fluid Power Mechatronics (FPM)*, Harbin, China, 2015, pp. 610–617.
- [23] M. S. Masmoudi, N. Krichen, M. Masmoudi, and N. Derbe, "Fuzzy logic controllers design for omnidirectional mobile robot navigation," *Appl. Soft Comput.*, vol. 49, pp. 901–919, Dec. 2016.
- [24] M. Pena et al., "Fuzzy logic for omni directional mobile platform control displacement using FPGA and Bluetooth," *IEEE Int. Latin Amer. Trans.*, vol. 13, no. 6, pp. 1907–1914, Jun. 2015.
- [25] C. Treesatayapun and A. C. Guzman-Carballido, "Linearization based on fuzzy rules emulated networks for nonaffine discrete-time systems controller," in *Proc. TENCON IEEE Region 10 Conf.*, Singapore, Jan. 2009, pp. 1–6.
- [26] R. H. Abiyev and O. Kaynak, "Identification and control of dynamic plants using fuzzy wavelet neural networks," in *Proc. Process. IEEE Int. Symp. Intell. Control*. San Antonio, TX, USA: CE Press, Sep. 2008, pp. 31–37.
- [27] K. Watanabe, Y. Shiraishi, S. G. Tzafestas, J. Tang, and T. Fukuda, "Feed-back control of an omnidirectional autonomous platform for mobile service robots," *J. Intell. Robot. Syst.*, vol. 22, nos. 3–4, pp. 315–330, 1998.
- [28] E. Hashemi, M. G. Jadidi, and N. G. Jadidi, "Model-based PI-fuzzy control of four-wheeled omni-directional mobile robots," *Robot. Auto. Syst.*, vol. 59, pp. 930–942, Nov. 2011.
- [29] S. W. Golomb, *Polyominoes—Puzzles, Patterns, Problems, and Packings*. Princeton, NJ, USA: Princeton Univ. Press, 1996.
- [30] C. Larson, "Combinatorial properties of polyiamonds," Ph.D. dissertation, Dept. Math., City Univ. New York, New York, NY, USA, 2014.
- [31] J. J. Parmar and C. V. Savant, "Selection of wheels in robotics," *Int. J. Sci. Eng. Res.*, vol. 5, no. 10, pp. 339–343, Oct. 2014.
- [32] *Robot Dynamics*. [Online]. Available: [http://www.societyofrobots.com/mechanics\\_dynamics.shtml#acceleration](http://www.societyofrobots.com/mechanics_dynamics.shtml#acceleration)
- [33] S. Böttcher, "Principles of robot locomotion," in *Proc. Hum. Robot Interact. Seminar*, 2006, pp. 1–25.
- [34] B. Adhikari, "Strength and failure mechanism in 3D printed parts," M.S. thesis, Dept. Mech. Mater., Aalto Univ. School Eng., Helsinki, Finland, 2016.
- [35] V. Nagarajan, A. K. Mohanty, and M. Misra, "Perspective on polylactic acid (PLA) based sustainable materials for durable applications: Focus on toughness and heat resistance," *ACS Sustain. Chem. Eng.*, vol. 4, no. 6, pp. 2899–2916, 2016, doi: [10.1021/acssuschemeng.6b00321](https://doi.org/10.1021/acssuschemeng.6b00321).
- [36] S. Sahu, B. B. Choudhury, and B. B. Biswal, "A vibration analysis of a 6 axis industrial robot using FEA," *Mater. Today-Proc.*, vol. 4, no. 2, pp. 2403–2410, 2017.
- [37] K. Dandan, A. Ananiev, I. Publication, and I. Kalaykov, "Dynamical analysis of silo surface cleaning robot using finite element method," *Int. J. Mech. Eng. Technol.*, vol. 7, no. 1, pp. 190–202, Jan./Feb. 2016.
- [38] J. H. Davis and J. R. Cogdell, "Calibration program for the 16-foot antenna," *Elect. Eng. Res. Lab.*, Univ. Texas, Austin, TX, USA, Tech. Memo. NG 006-69-3, Nov. 1987.



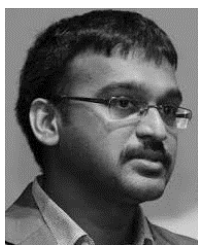
**RIZUWANA PARWEEN** received the bachelor's and master's degrees in mechanical engineering from the National Institute of Technology at Rourkela, India, and the Ph.D. degree from the Indian Institute of Science, Bangalore, India. She has over two years of industrial experience as a Product Development Engineer with KSB Tech Private Ltd., Pune, India, and as a Structural Analyst with CUMMINS, Pune. She was a Post-Doctoral Research Fellow with the Singapore University of Technology and Design (SUTD), where she worked on the design and development of Unloader Knee Brace for Asian Patients, in collaboration with physicians in Changi General Hospital, Singapore. She is currently a Research Fellow with the Engineering Product Development Pillar, SUTD, and is working on the design, development, and modeling of the self-reconfigurable floor cleaning robots.



**VEERAJAGADHESWAR PRABAKARAN** received the bachelor's degree in electronics and instrumentation engineering from Sathyabama University, India, in 2013, and the master's degree in information technology from Sikkim Manipal University, in 2016. He is currently a Research Assistant with the Temasek Laboratory, Singapore University of Technology and Design. He is also a Visiting Instructor for a design course of the International Design Institute, Zhejiang University, China. His research interest includes the development of complete coverage path planning, and SLAM frame work and embedded control for reconfigurable robots. He was a recipient of the SG Mark Design Award, in 2017, for the designing of h-Tetro and a self-reconfigurable cleaning robot.



**AYYALUSAMI VENGADESH** received the bachelor's degree from Sathyabama University, India, in 2013, and the master's degree in avionics from Anna University, India, in 2015. He is currently a Visiting Fellow with the Singapore University of Technology and Design under the supervision of Dr. M. R. Elara. His research interest focuses on the system modeling and designing of reconfigurable robots.



**MOHAN RAJESH ELARA** received the B.E. degree from the Amrita Institute of Technology and Sciences, Bharathiar University, India, and the M.Sc. degree in consumer electronics and the Ph.D. degree in electrical and electronics engineering from Nanyang Technological University, Singapore. He was a Lecturer with the School of Electrical and Electronics Engineering, Singapore Polytechnic. He is currently an Assistant Professor with the Engineering Product Development Pillar, Singapore University of Technology and Design. He is also a Visiting Faculty Member with the International Design Institute, Zhejiang University, China. He has published more than 80 papers in leading journals, books, and conferences. His research interests are in robotics with an emphasis on self-reconfigurable platforms and research problems related to robot ergonomics and autonomous systems. He was a recipient of the Tan Kah Kee Young Inventors' Award, in 2010, ASEE Best of Design in Engineering Award, in 2012, the SG Mark Design Award, in 2016, 2017, and 2018, and A' Design Award, in 2018. He has served in various positions for organizing and technical committees of over 20 international competitions and conferences.



**VINU SIVANANTHAM** received the B.Tech. degree in electronics and communication engineering from Amrita University, in 2017. From 2015 to 2017, he was a Junior Research Assistant with HuT Labs, where he was working on mechatronics and software development. He is currently a Visiting Fellow with the Singapore University of Technology and Design, where he is working on the mechatronics and software development of reconfigurable robots.

...